

pubs.acs.org/JCTC Article

Electronic Couplings versus Thermal Fluctuations in the Internal Conversion of Perylene Diimides: The Battle to Localize the Exciton

Published as part of Journal of Chemical Theory and Computation virtual special issue "First-Principles Simulations of Molecular Optoelectronic Materials: Elementary Excitations and Spatiotemporal Dynamics".

Nicolas Oldani, Victor M. Freixas, Dianelys Ondarse-Alvarez, Sahar Sharifzadeh, Tammie Gibson, Sergei Tretiak, and Sebastian Fernandez-Alberti*



Cite This: J. Chem. Theory Comput. 2024, 20, 5820-5828



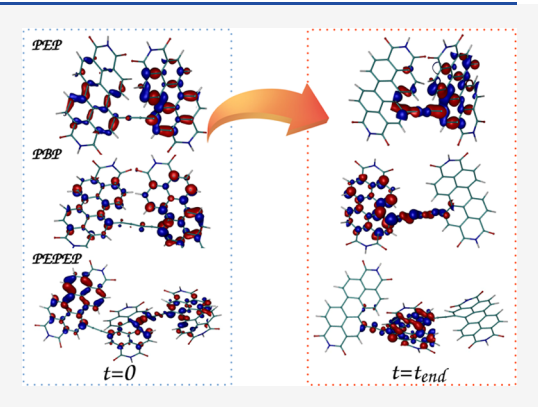
ACCESS

Metrics & More

Article Recommendations

S Supporting Information

ABSTRACT: Energy transfer processes among units of light-harvesting homooligomers impact the efficiency of these materials as components in organic optoelectronic devices such as solar cells. Perylene diimide (PDI), a prototypical dye, features exceptional light absorption and highly tunable optical and electronic properties. These properties can be modulated by varying the number of PDI units and linkers between them. Herein, atomistic nonadiabatic excited state molecular dynamics is used to explore the energy transfer during the internal conversion of acetylene and diacetylene bridged dimeric and trimeric PDIs. Our simulations reveal a significant impact of the bridge type on the transient exciton localization/delocalization between units of PDI dimers. After electronic relaxation, larger exciton delocalization occurs in the PDI dimer connected by the diacetylene bridge with respect to the one connected by the shorter acetylene bridge. These changes can be rationalized by the Frenkel



exciton model. We outline a technique for deriving parameters for this model using inputs provided by nonadiabatic dynamics simulations. Frenkel exciton description reveals an interplay between the relative strengths of the diagonal and off-diagonal disorders. Moreover, atomistic simulations and the Frenkel exciton model of the PDI trimer systems corroborate in detail the localization properties of the exciton on the molecular units during the internal conversion to the lowest-energy excited state when the units become effectively decoupled. Overall, atomistic nonadiabatic simulations in combination with the Frenkel exciton model can serve as a predictive framework for analyzing and predicting desired exciton traps in PDI-based oligomers designed for organic electronics and photonic devices.

1. INTRODUCTION

The efficiency of energy transfer among units of light-harvesting systems is a major factor defining their application in organic optoelectronic devices. In these materials, the electronic density localization is concomitant to the exciton displacement by funneling the initial excess of electronic energy deposited upon photoabsorption, replicating the fundamental physical mechanisms that play in natural light-harvesting complexes. Moreover, these processes often depend on the specific covalent molecular linker that binds the chromophore units together. ^{2–5}

Perylene diimide (PDI)-based oligomers feature highly efficient light absorption and tunable optical and electronic properties^{6–11} resulting in their applications¹² as materials for organic light emitting devices, organic field effect transistors, and organic solar cells, building blocks for functional supramolecular architectures, and nonfullerene materials among others. ^{13–24} Studies of excited state dynamics of PDI-related organic compounds in thin films provide important

insights into the exciton formation and decay dynamics, revealing that initial photoinduced delocalized excitons experience ultrafast exciton decay within hundreds of femtoseconds into spatially confined trap sites. ²⁵ Moreover, PDI oligomers have been intensely studied, as the different association motifs and morphologies influence the optical and electronic properties. ^{4,26} Experimental and theoretical studies performed on PDI-based materials and oligomers have also analyzed how structural geometry relaxation and flexibility at ambient temperatures counteract initial exciton delocalization. ^{27–29} Spectroscopic properties of PDI-based materials can be modulated by introducing different substitution patterns or

Received: April 12, 2024 Revised: June 28, 2024 Accepted: July 1, 2024 Published: July 10, 2024





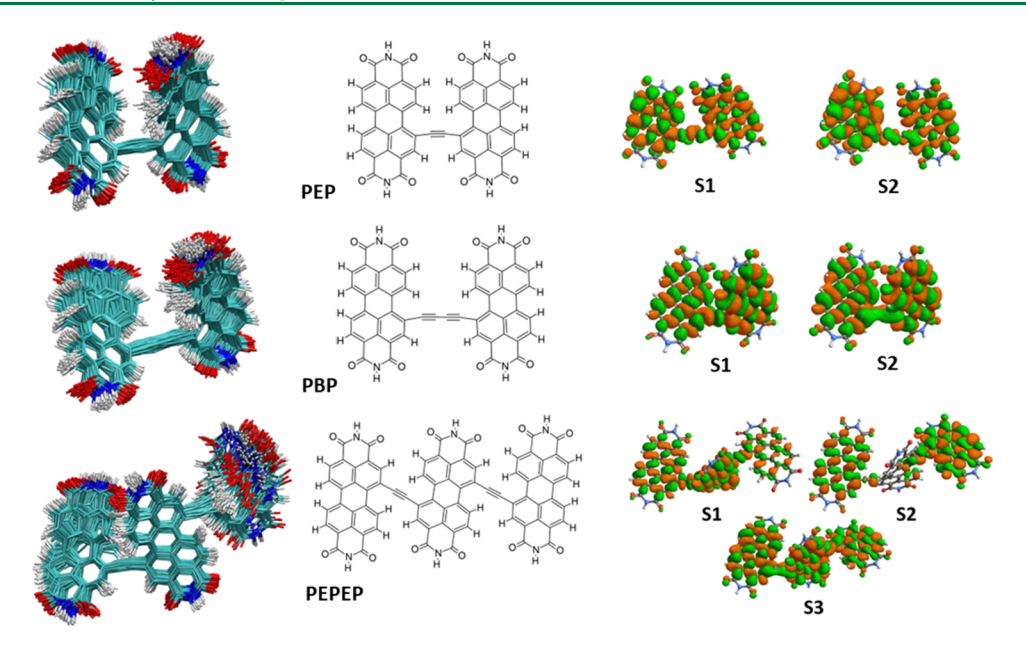


Figure 1. Chemical structures and superposition of snapshots obtained from exploration of the conformational space during ground-state molecular simulations of PEP, PBP, and PEPEP at 300 K. The corresponding spatial distribution of electronic transition densities of S_1 , S_2 , and S_3 (only for the trimer), calculated for the ground-state energy minimum, is also shown.

using different linkers connecting PDI units.^{30–33} Effects of conformational disorder, solvation, energy, and charge-transfer excitations on absorption spectrum and photoinduced dynamics of PDI monomers and dimers have been previously explored using a linear vibronic coupling (LVC) Hamiltonians.^{34,35}

In previous works, we studied the effect of stacking in the electronic and vibrational relaxation of PDI monomers, ³⁶ dimers, ³⁷ and trimers ³⁸ by means of nonadiabatic excited state molecular dynamics using the NEXMD software package. ^{39,40} Our studies revealed an acceleration of the nonradiative relaxation with the number of stacked PDI units due to a combination of decreasing the energy gaps between electronic excited states and the activation of a positive feedback mechanism involving a common set of vibrational normal modes that accelerate the process by increasing the efficiency of vibronic dynamics. The two mechanisms create a synergistic effect that eliminate transient accumulation of electronic populations in intermediate electronic excited states.

These modeled systems tend to form stack-like configurations. Other topological configurations have been investigated as well. For example, previous experimental works^{4,26,41,42} explored optical properties and excited state dynamics of ethynylene (i.e., acetylene-)- and butadiynylene (i.e., diacetylene-)-bridged dimeric (named PEP and PBP, respectively) and trimeric (PEPEP) PDIs (see Figure 1) by using ultrafast transient absorption, two-dimensional electronic spectroscopy (2DES), and single-molecule spectroscopy. These probes inspected the interplay between electronic coherences and energy equilibration, indicating that radiationless transitions that take place in the initial strong electronic coupling regime within the excitonic manifold after photoexcitation occur at very early times (<50 fs), precluding the persistence of long-lived coherences. Herein, we explore in detail the intramolecular energy transfer during the internal conversion of PEP, PBP, and PEPEP using NEXMD simulations, emphasizing changes in the spatial localization/ delocalization of the electronic transition densities. We parallel atomistic simulations with the analysis of the emerging electronic structure using an intuitive Frenkel exciton model^{34-51} framework that relies on the inputs provided by NEXMD simulations.

2. RESULTS AND DISCUSSION

The photodynamics of PEP, PBP dimers, and PEPEP trimer of PDI, shown in Figure 1, have been simulated. Figure 1 also shows the superposition of snapshots obtained from exploration of the conformational space sampled during ground-state molecular simulations, which are used as initial structures for the subsequent NEXMD simulations. Thermal fluctuations present oscillations around one major cisoid isomer, consistent with previous theoretical and experimental studies. 41 The corresponding spatial distribution of electronic transition densities of S_1 and S_2 (and also S_3 for the trimer), calculated for the ground-state energy minimum, is also shown. We can notice the antisymmetric and symmetric characters S₁ and S2 for PEP and PBP dimers as an inversion of the transition density phase in one of the monomers, which is in accordance with the Frenkel exciton model (see eq 5 in the Section 4). Also, there are no contributions from the middle monomer to S_2 in the trimer (see eq 12 in Section 4).

For each system, the simulated absorption spectra, showing the individual contributions of selected excited states, are shown in Figure 2(a). In good agreement with previous experimental works, $^{4,26,41,42}_{,4,26,41,42}$ the absorption spectrum of the PDI dimers is a superposition of S_1 and S_2 state absorptions, which are antisymmetric and symmetric superpositions of the monomer excitations for perfectly symmetric configurations. Thermal fluctuations, however, might break this symmetry, localizing the exciton in one of the monomers. The calculated fwhm of the corresponding associated absorption bands of S_1 and S_2 states is ~ 0.16 eV either for PEP or PBP, indicating equivalent strengths of the thermal fluctuations for both dimers. Further analysis of the flexibility between both dimers can be performed by analyzing variations of the dihedral angle connecting the PDI units during the excited state molecular

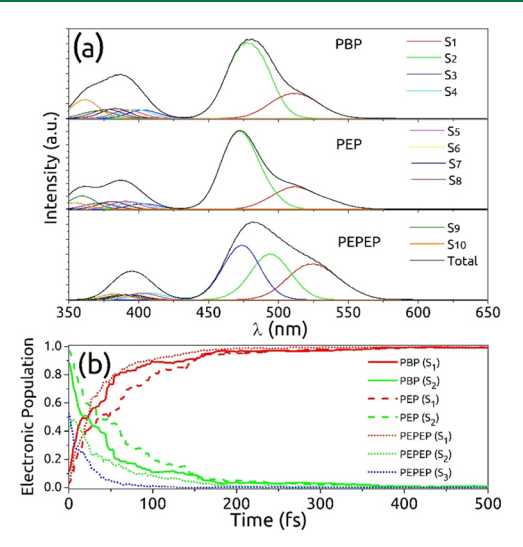


Figure 2. (a) Simulated absorption spectra showing the individual contributions of selected excited states; (b) evolution of average populations of excited states with time for the simulation of the trajectory ensembles.

dynamics simulations. Supporting Figure S1 shows the evolution of these dihedral angles for PEP, PBP, and PEPEP. Values of 44 ± 10 and $55 \pm 17^{\circ}$ are obtained for PEP and PBP, respectively, indicating that PBP exhibits slightly more flexible torsional motions between PDI units with respect to PEP, as expected due to the larger bridge (and thus less steric hindrance) connecting both PDI units. As we point out later, the smaller average dihedral angle of PEP with respect to PBP contributes to a further delocalization of its wave function between both PDI units. This agrees with the fluorescence dynamics monitored by single-molecule fluorescence spectroscopy,⁴ which reveals fluctuations in the fluorescence signal of PBP caused by conformational changes of the molecule due to the enhanced flexibility endowed by the longer butadiynylene linker. Moreover, the smaller average dihedral angle of PEP contributes to the delocalization of its wave function between both PDI units. Besides, larger energy gaps between absorption bands associated with S₁ and S₂ states are observed for PEP with respect to PBP, i.e., $\Delta E_{1-2} = 0.206$ and 0.168 eV, respectively. Larger electronic coupling leads to the larger ΔE_{1-2} , and the resultant S₁ and S₂ electronic states become closer to the perfect symmetric and antisymmetric combinations, being effectively more electronically delocalized, as shown in Figure 1. Our calculation of the corresponding natural transition orbitals for the different excited states, as shown in Supporting Figure S5, indicates the absence of charge-transfer character in these states. As we describe later, further competition between electronic coupling and thermal fluctuations will affect the exciton delocalization. Finally, in agreement with experimental steady-state absorption spectra, the S2 bands for PEP and PEPEP are equivalent, while it is slightly red-shifted for PBP.

The evolutions of electronic state populations obtained from the NEXMD simulations of PEP, PBP, and PEPEP are shown in Figure 2(b). According to the contributions to the absorption band at the initial laser photoexcitation wavelength, the distribution of initially excited states was S_1 (11%) and S_2 (89%) for PBP, S_1 (3%) and S_2 (97%) for PEP, and S_1 (6%), S_2 (41%), and S_3 (53%) for PBP, and S_1 (3%) and S_2 (97%) for PEP with no contributions from higher energy states. In

previous works, we have reported that an increase in the number of stacked PDI units noticeably accelerates energy decay.³⁸ In that case, excitations were performed to the upper energy band (~406 nm), and the increase of the population in the lowest-energy S₁ state was modulated by the slow relaxation from higher-energy electronic states, i.e., slow energy relaxation of S₃ and S₄ for the PDI dimer and trimer, respectively. Herein, excitations are performed at the lower energy band (~480 nm), so the upper energy band is not initially populated. Therefore, here, we focus on the $S_2 \rightarrow S_1$ and $S_{2/3} \rightarrow S_1$ internal conversion processes for PDI dimers and trimers, respectively, where significantly faster relaxation times are observed. In our computational studies, higherenergy electronic states are not initially populated. Even though up to 10 electronic states are explicitly included in simulations, high energy states do not participate in the nonadiabatic relaxation processes. Moreover, as it has been pointed out in previous experimental works,⁴¹ the ultrafast internal conversion process cannot be explained by coupling to a solvent spectral density. The large number of internal vibrational degrees of freedom in combination with the time scale of the internal conversion processes observed and the degree of exciton delocalization induces a vibrational redistribution that makes the molecule to actually act as its own bath. At this point, it is important to stress that, according to Frenkel exciton model, an ideal trimeric system could also be arranged such that the couplings between all monomers are the same $(V = V_1 = V_2 \text{ eqs } 11 \text{ and } 12 \text{ in the Section } 4)$, so S_1 and S2 states would degenerate. This is not the case in our study, where the trimer is arranged in such a way that the coupling between the two further away monomers is smaller than the coupling between the adjacent ones. So, herein, we are analyzing relaxation through the gap mediated by electronic coupling between monomers.

PEP relaxes slower than PBP and PEPEP, indicating that a larger bridge connecting PDI units and/or an increase of units (as in the PEPEP case) accelerates the internal conversion process. Actually, the initial nonadiabatic coupling terms (NACT) between S₁ and S₂ states are larger in PBP and PEPEP with respect to PEP (see Supporting Figure S2). In agreement with experimental results, ⁴¹ the ultrafast internal conversion processes are 2 orders of magnitude faster than bath-mediated processes, indicating that the intramolecular degrees of freedom dominate this process, and the solvent effect can be neglected.

The exciton spatial localization on each PDI unit can be evaluated using the fraction of transition density, δ_x^{α} , localized on each of them (eq 1 in the Section 4). Figure 3(a) shows the distribution density of δ_x^{α} at initial t_0 and final $t_{\rm end}$ times of NEXMD simulations. We can observe that, initially, excitations for both PEP and PBP dimers are significantly delocalized between the individual PDI units, with PEP being more delocalized than PBP. That is, both dimers present significant probabilities of $\delta_x^{\alpha} \sim 0.5$, indicating that the exciton is delocalized between both PDI units. This is in agreement with the substantial electronic coupling between PDI units predicted by the exciton splitting reported in the experimental⁴¹ and simulated absorption spectra (Figure 2(a)) and initial nonadiabatic couplings between S₁ and S₂ states (Supporting Figure S2). Furthermore, the strong nonadiabatic coupling regime is responsible for the ultrafast internal conversion process that takes place after photoexcitation and the experimentally reported absence of persistence of long-

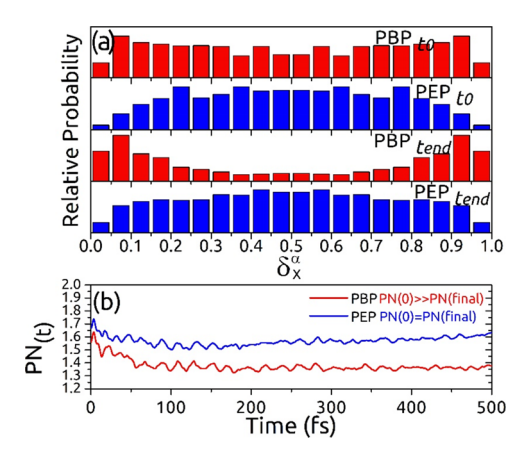


Figure 3. (a) Fraction of transition density, δ_x^{α} , localized on each PDI unit collected at initial (t_0) and final $(t_{\rm end})$ times during excited state dynamics; (b) time evolution of the average over all trajectories of participation number PN(t).

lived coherences between S_1 and S_2 states observed in two-dimensional electronic spectroscopy. The excited state dynamics localize the exciton in one PDI unit of PBP, revealed as high peaks at $\delta_x^{\alpha} \sim 0$ and 1 with a low contribution of $\delta_x^{\alpha} \sim 0.5$ at $t_{\rm end}$. In contrast, the exciton remains delocalized in PEP.

The extent of the exciton (de)localization within the PDI dimers can be monitored by the monomer participation number PN(t), which varies between 1 and 2 (eq 2 in the Section 4). Figure 3(b) shows the time evolution of the average PN(t) during excited state dynamics of PEP and PBP. We observe that the excited state dynamics spatially localize the exciton in one monomer of PBP, while this is not the case for PEP. In both cases, an ultrafast transient localization at ~100 fs takes place. This can be explained by the effect of a transient increase of the relative strength of thermal fluctuations due to the initial excess of kinetic energy transferred to vibrational degrees of freedom coupled to the electronic system immediately after photoexcitation. With subsequent equilibration in the vibrational system, an excitation in PEP becomes slightly more delocalized, matching an initial point of the dynamics. In contrast, PBP excitation remains more localized in the subsequent dynamics. According to the stabilized asymptotic values of PN(t) at the final times of our simulations, further changes in the extent of the exciton (de)localization within the PDI dimers are not expected.

The Frenkel exciton model allows us to intuitively rationalize an interplay between off-diagonal disorder (V fluctuations) between PDI units and their diagonal disorder (Δ). The relative values of V modulate the exciton spatial localization. Following the procedure described in the Section 4, values of V and Δ have been evaluated from NEXMD simulations. Figure 4(a,b) shows the average values of Δ at initial t_0 and final $t_{\rm end}$ times of NEXMD simulations. We observe that both PBP and PEP dimers show very similar values of Δ . Due to the excess of kinetic energy transferred to the vibrational system after 500 fs, Δ values are generally becoming larger at $t_{\rm end}$ with respect to t_0 . The width of the distributions increases as well.

Figure 4(c,d) shows the distribution of electronic couplings V averaged at initial t_0 and final $t_{\rm end}$ times of NEXMD simulations. As expected, changes in the distributions are related to the minimal conformational changes during the excited state dynamics. As it is expected, values of V are around

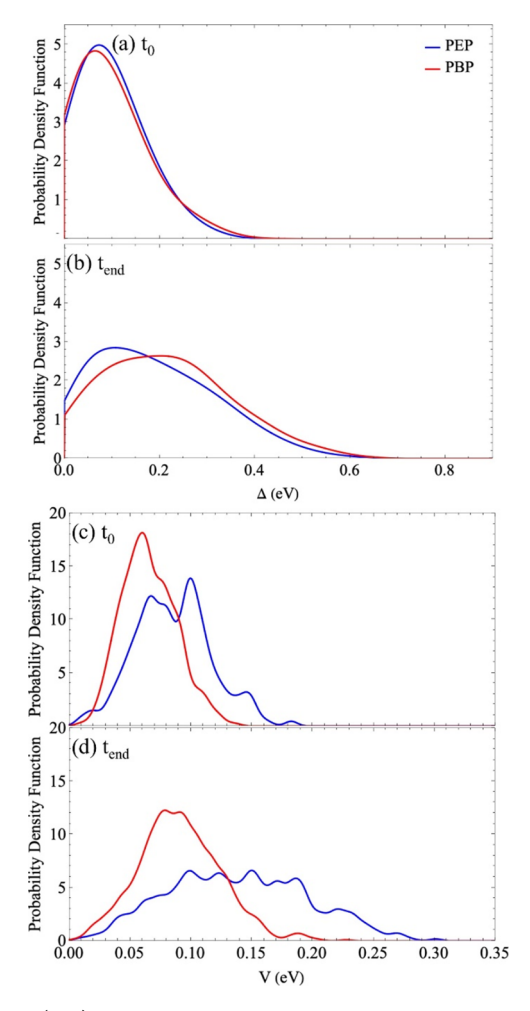


Figure 4. (a, b) Probability densities of diagonal disorder Δ and (c, d) off-diagonal disorder V at initial t_0 and final $t_{\rm end}$ for PEP and PBP dimers.

 \sim 0.12 eV that correspond to the difference between the peaks assigned to S₁ and S₂ states in the absorption spectra, as shown in Figure 2(a). The couplings between PDI units are persistently larger in PEP with respect to PBP. This is also expected since the length of the bridge in PEP is shorter than that in PBP. At this point, it is worth pointing out that while the electronic coupling between PDI units (V) is larger in PEP with respect to PBP, nonadiabatic coupling terms (NACT) have the opposite behavior, being larger in PBP than in PEP. This can be easily explained since, according to the Frenkel exciton model, for $\Delta = 0$, $V = \frac{E_2 - E_1}{2}$, while NACT_{1,2}, calculated during NEXMD simulations, is inversely proportional to the gap, $E_2 - E_1$.

The degree of exciton delocalization/localization between PDI units can be calculated according to the Frenkel exciton model using values of DL (see eq 9 in the Section 4). Figure 5 shows the probability density function of DL at initial t_0 and final $t_{\rm end}$ times of NEXMD simulations. In agreement with Figure 3, both PEP and PBP present high levels of delocalization at t_0 . Nevertheless, while PBP becomes more localized at $t_{\rm end}$, PEP remains delocalized due to its larger off-diagonal V. That is, a minimalistic Frenkel exciton model provides a straightforward theoretical model, which is able to describe exciton localization/delocalization in these systems. Furthermore, the interplay between the off-diagonal disorder

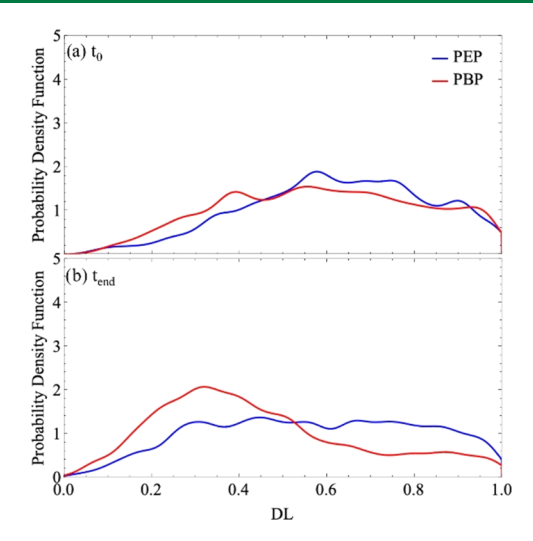


Figure 5. Probability densities of exciton localization/delocalization (DL) according to the Frenkel exciton model for PEP and PBP at (a) initial t_0 and (b) final $t_{\rm end}$ times.

and the diagonal disorder Δ determines the exciton delocalization between PDI units (see eq 9 in the Section 4), being more delocalized for larger values of V and smaller values of Δ .

In the case of the PDI trimer, the distribution of off-diagonal disorders V_1 and V_2 at initial t_0 and final $t_{\rm end}$ times of NEXMD simulations is shown in Figure 6. Here, it is important to notice

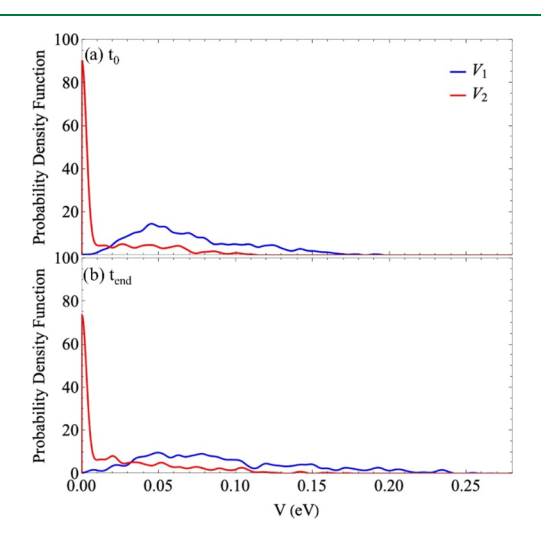


Figure 6. Probability densities of off-diagonal disorders V_1 and V_2 at (a) initial t_0 and (b) final $t_{\rm end}$ for PDI trimer.

that V_1 represents the electronic couplings between adjacent PDI units, which is in general different for each pair due to the presence of the thermal fluctuation-induced off-diagonal disorder. These values are obtained as described in the Section 4. As it is expected, significantly larger values of V_1 with respect to V_2 are observed, indicating that the couplings between nearest PDI units (V_1) are larger than the coupling between next-to-nearest units (V_2) , and the neglect of these latter can be considered within a good approximation level. At this point, it is important to notice that these values of coupling are consistent with those obtained in experimental measurements for PDI oligomers 53,54 and belong to the weak-to-intermediate

coupling regime, allowing the interplay with thermal fluctuations to localize the exciton.

The energy redistribution across the PDI trimer can be monitored by evaluating the evolution of the fraction of transition density, δ_x^{α} , localized in the middle PDI unit and in the two outermost units together. Figure 7 shows an effective

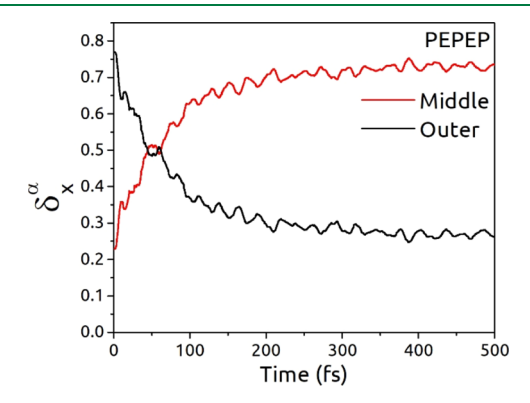


Figure 7. Time evolution of the average over all trajectories of the fraction of transition density, δ_x^a , localized in the middle PDI unit and in the outer ones.

outer → middle exciton redistribution. The final localization in the middle unit is in agreement with the Frenkel exciton model for the minimum energy configuration (see the Section 4), for which the wave function for the S₁ state is more localized in the middle unit than in the outer ones. Once the system has relaxed to the lowest-energy excited state (S_1) and the units become decoupled, we can consider $V_2 \sim 0$. The final values of $\delta_x^{\alpha} \sim 0.7$ in the middle PDI unit and ~ 0.3 in the outer PDI units can be further analyzed in Figure S3, where we can observe that actually most of the trajectories finish with 70% of their transition density localized in the middle unit and 30% in the outer unit. The analysis of energy transfers through the different pathways can be performed using the transition density flux method^{52,55} (see Supporting Information Transition Density Flux Analysis Section). Supporting Figure S4 shows that there is a negligible outer → outer density flux, i.e., direct through-space energy transfer between the two outer PDI units bypassing the middle one is essentially suppressed.

3. CONCLUSIONS

The intramolecular energy redistribution after photoexcitation of PEP and PBP dimers and PEPEP trimer of PDI has been analyzed using atomistic nonadiabatic excited state molecular dynamics (NEXMD) simulations combined with the Frenkel exciton model. The initial strong coupling regime, which accounts for the experimentally observed inhibition of long-lived coherences, is confirmed in our simulations by the high degree of initial exciton delocalization observed in both dimers. Besides, the analysis of the exciton spatial delocalization/localization reveals a significant impact of the different types of bridge between PEP and PBP dimers, which modulates the resulting electronic couplings.

As a result, the interplay between the relative strengths of the thermal fluctuations and couplings is responsible for this delocalization/localization difference. The Frenkel exciton model, incorporating information provided by dynamical NEXMD simulations, shows a larger off-diagonal disorder in PEP compared to PBP.

NEXMD simulations and the Frenkel exciton model of the PDI trimer agree in the final localization of the exciton on the middle monomer, once the system has relaxed to the lowest-energy excited state (S_1) . The PDI trimer experiences an efficient outer-to-middle energy transfer between PDI units with a negligible through-space transfer between the outer units.

Atomistic NEXMD simulations produce detailed information on nonradiative relaxation and energy transfer processes. In this contribution, we have exemplified how to map this information into the Frenkel exciton framework, a commonly used reduced description of the electronic structure of multichromophoric systems. We show how complex dynamical information can be used to derive the distribution of electronic couplings between individual chromophores and the effects of thermal fluctuations present in a given system. These provide convenient means to analyze an interplay between these two factors and connect it to the localization and delocalization properties of electronic wave functions. Overall, nonadiabatic simulations in combination with the Frenkel exciton model allow us to achieve a complete description of exciton properties, interunit energy transfer, couplings, and spatial localization useful to be extended to other oligomers designed for organic electronics and photonic devices.

4. METHODS

4.1. Nonadiabatic Excited State Molecular Dynamics.

Photoexcitation and electronic energy relaxation and redistribution of ethynylene (PEP)- and butadiynylene (PBP)bridged dimeric (PEPEP) PDIs, as shown in Figure 1, have been simulated using the NEXMD package. 39,40 The NEXMD code performs direct nonadiabatic excited state molecular dynamics simulations, making use of different hybrid quantumclassical methods, namely, trajectory surface hopping (TSH), Ehrenfest dynamics (EHR), and the ab initio multiple cloning sampling technique for multiconfigurational ehrenfest quantum dynamics (MCE-AIMC). Herein, only the TSH method is used to balance accuracy and computational efficiency. The use of NEXMD to simulate photoinduced dynamics of PDI aggregates has been validated in our previous studies.^{36–38} The configuration interaction singles (CIS) level in combination with the Hamiltonian AM1⁵⁶ provides a semiquantitative description for excited states in these systems as compared to experiments and higher-level electronic structure simulations.

4.2. Analyses of Transient Exciton Localization. The spatial localization of electronic excitations can be monitored throughout the NEXMD simulations by calculating the evolution in time of the respective transition density matrices. These quantities are given in the atomic orbital (AO) basis as $(\rho^{0\alpha})_{ij} = \langle \phi_{\alpha} | c_i^{\dagger} c_j | \phi_0 \rangle$, with ϕ_0 and ϕ_{α} being the wave functions corresponding to the adiabatic ground and excited states, respectively, c_i^{\dagger} and c_j are the respective creation and annihilation operators acting over AO i and j. The diagonal element $(\rho^{0\alpha})_{ii}$ is relevant to the change in the net charge of the electronic density on AO i during a transition from the ground to the excited states α . Consequently, the fraction of $\rho^{0\alpha}$ localized on a specific PDI unit x is defined as

$$\delta_x^{\alpha} = (\rho^{0\alpha})_x^2 = \sum_{i \in x} (\rho^{0\alpha})_{ii}^2$$
 (1)

with $\rho^{0\alpha}$ renormalized as $\frac{\rho^{0\alpha}}{\sum_{x=1,n}\delta_x^{\alpha}}$, where n represents the total number of monomers in the oligomer. The extent of the exciton (de)localization within the oligomer can be monitored by defining the monomer participation number as

$$PN(t) = [(\delta_x^{\alpha}(t))^2]^{-1}$$
 (2)

PN(t) ranges from n for a completely delocalized exciton to 1 for an exciton located on a single monomer unit.

4.3. NEXMD Computational Details. For each molecule, 2 ns equilibrated ground-state dynamics simulations, using the Langevin equation at 300 K with a friction coefficient $\gamma = 20$ ps⁻¹, are used to collect 400 snapshots, equally spaced in time every 2.5 ps after neglecting the first 1 ns of equilibration. These configurations serve as initial conditions for subsequent NEXMD simulations of PEP, PBP, and PEPEP (Figure 1). The exploration of the conformational space can be visualized by the superposition of these snapshots as shown in Figure 1. Absorption spectra are modeled from these initial configurations by collecting vertical excitation energies of the 10 lowest excited states and their oscillator strengths. The initial photoexcitations for NEXMD simulations are simulated by a vertical laser excitation to an initial state, selected according to their oscillator strengths, using a Franck-Condon window simulating a Gaussian laser pulse with fwhm = 100 fs centered at 470, 480, and 480 nm for PEP, PBP, and PEPEP, respectively. Classical time steps of 0.5 and 0.1 fs are used for the propagation of nuclei in the ground and excited state trajectories, respectively. Six excited states are included in the simulations. More details about NEXMD simulations and relevant typical parameters can be found in our previous works.²⁶

4.4. Frenkel Exciton Models. The Frenkel exciton model can be used to analyze the localization/delocalization of excited states during the internal conversion process in PDI dimers. S_1 and S_2 states of the dimer are expressed as linear combinations of the S_1 state of each monomer with a transition energy E and off-diagonal elements V, i.e., variance in V, represent the electronic coupling between chromophores. The Frenkel exciton Hamiltonian matrix for PDI dimers is given by

$$H = \begin{pmatrix} E & V \\ V & E \end{pmatrix} \tag{3}$$

with eigenvalues

$$E_{S_{1/2}} = E \pm V \tag{4}$$

and eigenvectors

$$X_{S_{1/2}} = (\pm 1, 1) \tag{5}$$

i.e., S_1 and S_2 states are the antisymmetric and symmetric superpositions of the monomer solutions.

In realistic systems, disorder modulates the energy E of individual monomers, and S_1 and S_2 states of the dimer are no longer perfectly antisymmetric and symmetric superpositions of the monomer solutions, leading in some cases to a complete localization of the dimer wave function in one of the monomers. In order to mimic the conditions that favor the localization of the dimer wave function, the variance of diagonal elements Δ , i.e., the diagonal disorder, can be introduced, and H can be rewritten as

$$H = \begin{pmatrix} E + \Delta & V \\ V & E \end{pmatrix} \tag{6}$$

which has eigenvalues

$$E_{S_{1/2}} = \frac{1}{2} (2E + \Delta \mp \sqrt{\Delta^2 + 4V^2})$$
 (7)

and eigenvectors

$$X_{S_{1/2}} = \left(\frac{\Delta \mp \sqrt{\Delta^2 + 4V^2}}{2V}, 1\right)$$
 (8)

When solving eq 7, one can define the degree of delocalization/localization DL as

$$DL = \frac{\Delta + \sqrt{\Delta^2 + 4V^2}}{2V} = \sqrt{\frac{E - E_{S_1}}{E_{S_2 - E}}}$$
(9)

with $(E_{S_1} < E < E_{S_2})$. DL varies between 0 and 1, where lower values correspond to a wave function that is more localized on one individual monomer.

All essential ingredients of the Frenkel exciton model can be obtained from NEXMD simulations. For example, E_{S_1} and E_{S_2} correspond to the transition energies of the two lowest excited states of the aggregate (i.e., the PDI dimer during NEXMD simulations), whereas the values of E and Δ can be obtained by calculating the energy values of E for isolated monomers (where the bridge is removed from the structure). Using eq 7, $V = \frac{1}{2}\sqrt{(E_{S_2} - E_{S_1})^2 - \Delta^2}$ and the diagonal disorder Δ can be calculated as the difference between the E1 energies corresponding to the isolated PDI units, i.e., E3 energies corresponding to the isolated PDI units, i.e., E4 and E5 are the E5 energies calculated on the isolated PDI units A and B, respectively.

The Frenkel exciton Hamiltonian for PDI trimer in a perfectly symmetric configuration can be written as

$$H = \begin{pmatrix} E & V_1 & V_2 \\ V_1 & E & V_1 \\ V_2 & V_1 & E \end{pmatrix}$$
 (10)

where E is the on-site energy, i.e., the energy of the S_1 state of individual monomers, V_1 (V_{12} and V_{23}) are the nearest-neighbor electronic couplings, and V_2 (V_{13}) is the next-to-nearest electronic coupling. The corresponding eigenvalues are

$$\begin{split} E_{S_1} &= \frac{1}{2} (2E + V_2 - \sqrt{8V_1^2 + V_2^2}) \\ E_{S_2} &= E - V_2 \\ E_{S_3} &= \frac{1}{2} (2E + V_2 + \sqrt{8V_1^2 + V_2^2}) \end{split} \tag{11}$$

with E_{S_1} , E_{S_2} , and E_{S_3} are the energies corresponding, respectively, to S_1 , S_2 , and S_3 of the trimer. The corresponding eigenvectors are

$$\left(1, -\frac{V_2 + \sqrt{8V_1^2 + V_2^2}}{2V_1}, 1\right)$$

 $(-1 \ 0 \ 1)$

$$\left(1, -\frac{V_2 - \sqrt{8V_1^2 + V_2^2}}{2V_1}, 1\right)$$
(12)

As in the case of PDI dimers, all essential ingredients of the Frenkel exciton model can be obtained from NEXMD simulations. $E_{\rm S_1}$, $E_{\rm S_2}$, and $E_{\rm S_3}$ correspond to the transition energies of the three lowest excited states of the PDI trimer calculated from NEXMD simulations. V_1 is obtained by cutting the trimer in two dimers, each of them including the middle unit and one of the outer units, and removing the bridge with the third unit. Then, an equivalent procedure as it has been described for PDI dimers is performed. Once V_1 values are obtained (i.e., V_{12} and V_{23}), V_2 is calculated using the Hamiltonian

$$H = \begin{pmatrix} E_{S_1}^1 & V_{12} & V_2 \\ V_{12} & E_{S_1}^2 & V_{23} \\ V_2 & V_{23} & E_{S_1}^3 \end{pmatrix}$$
(13)

for each individual configuration collected from NEXMD simulations, where $E_{\mathrm{S}_1}^1$, $E_{\mathrm{S}_1}^2$, and $E_{\mathrm{S}_1}^3$ are the energies of the S_1 state for each monomer, and V_{12} and V_{23} are the couplings obtained solving from the Hamiltonian for each of the two dimers as it has been explained previously. The eigenvalues of H are calculated and compared to the energy values of S_1 , S_2 , and S_3 for the trimer to obtain the values of V_2 numerically.

ASSOCIATED CONTENT

Data Availability Statement

Program code, license, and documentation may be accessed at https://github.com/lanl/NEXMD.

Supporting Information

The Supporting Information is available free of charge at https://pubs.acs.org/doi/10.1021/acs.jctc.4c00486.

Frenkel exciton model for PDI trimer and the method for transition density flux analysis; the evolution of these dihedral angles and nonadiabatic coupling terms, respectively, for all systems (Figures S1 and S2); the fraction of transition density localized in the middle PDI unit and in the outer ones at final time during excited state dynamics (Figure S3); displays the accumulated transition density fluxes between outer and middle PDI units of the PDI trimer (Figure S4), and natural transition orbitals for the different excited states (Figure S5) (PDF)

AUTHOR INFORMATION

Corresponding Author

Sebastian Fernandez-Alberti — Departamento de Ciencia y Tecnologia, Universidad Nacional de Quilmes/CONICET, B1876BXD Bernal, Argentina; ⊙ orcid.org/0000-0002-0916-5069; Email: sfalberti@gmail.com

Authors

- Nicolas Oldani Departamento de Ciencia y Tecnologia, Universidad Nacional de Quilmes/CONICET, B1876BXD Bernal, Argentina
- Victor M. Freixas Department of Chemistry and Physics and Astronomy, University of California, Irvine, California 92697-2025, United States; orcid.org/0000-0003-1733-4827
- Dianelys Ondarse-Alvarez Departamento de Ciencia y Tecnologia, Universidad Nacional de Quilmes/CONICET, B1876BXD Bernal, Argentina
- Sahar Sharifzadeh Division of Materials Science and Engineering, Boston University, Boston, Massachusetts 02215, United States; orcid.org/0000-0003-4215-4668
- Tammie Gibson Theoretical Division, Center for Nonlinear Studies (CNLS), and Center for Integrated Nanotechnologies (CINT), Los Alamos National Laboratory, Los Alamos, New Mexico 87545, United States; orcid.org/0000-0002-3173-5291
- Sergei Tretiak Theoretical Division, Center for Nonlinear Studies (CNLS), and Center for Integrated Nanotechnologies (CINT), Los Alamos National Laboratory, Los Alamos, New Mexico 87545, United States; orcid.org/0000-0001-5547-3647

Complete contact information is available at: https://pubs.acs.org/10.1021/acs.jctc.4c00486

Notes

The authors declare no competing financial interest.

ACKNOWLEDGMENTS

S.T. acknowledges support from the U.S. DOE, Office of Science, Office of Basic Energy Sciences under Triad National Security, LLC ("Triad") contract grant #89233218CNA000001 (FWP: LANLE3T1). This work was performed in part at the Center for Integrated Nanotechnology (CINT) at Los Alamos National Laboratory (LANL), a U.S. DOE and Office of Basic Energy Sciences user facility. This research used resources provided by the LANL Institutional Computing Program. S.F.-A., D.O.-A., and N.O. acknowledge the support of CONICET and ANPCyT (PICT 2018-02360). S.S. acknowledges financial support from the National Science Foundation (NSF) CAREER program, under grant number DMR-1847774.

REFERENCES

- (1) Cao, S.; Rosławska, A.; Doppagne, B.; Romeo, M.; Féron, M.; Chérioux, F.; Bulou, H.; Scheurer, F.; Schull, G. Energy Funnelling within Multichromophore Architectures Monitored with Subnanometre Resolution. *Nat. Chem.* **2021**, *13*, 766–770.
- (2) Meier, H. Conjugated Oligomers with Terminal Donor-Acceptor Substitution. *Angew. Chem., Int. Ed* **2005**, 44, 2482–2506.
- (3) Patalag, L. J.; Ho, L. P.; Jones, P. G.; Werz, D. B. Ethylene-Bridged Oligo-BODIPYs: Access to Intramolecular J-Aggregates and Superfluorophores. *J. Am. Chem. Soc.* **2017**, *139*, 15104–15113.
- (4) Cho, J.-W.; Yoo, H.; Lee, J.-E.; Yan, Q.; Zhao, D.; Kim, D. Intramolecular Interactions of Highly π -Conjugated Perylenediimide Oligomers Probed by Single-Molecule Spectroscopy. *J. Phys. Chem. Lett.* **2014**, *5*, 3895–3901.
- (5) Rodríguez-Córdoba, W.; Sierra, C. A.; Puentes, C. O.; Lahti, P. M.; Peon, J. Photoinduced Energy Transfer in Bichromophoric Pyrene-PPV Oligomer Systems: The Role of Flexible Donor-Acceptor Bridges. *J. Phys. Chem. B* **2012**, *116*, 3490–3503.

- (6) Chiş, V.; Mile, G.; Ştiufiuc, R.; Leopold, N.; Oltean, M. Vibrational and Electronic Structure of PTCDI and Melamine—PTCDI Complexes. *J. Mol. Struct.* **2009**, 924–926, 47–53.
- (7) Oltean, M.; Calborean, A.; Mile, G.; Vidrighin, M.; Iosin, M.; Leopold, L.; Maniu, D.; Leopold, N.; Chiş, V. Absorption Spectra of PTCDI: A Combined UV-Vis and TD-DFT Study. *Spectrochim. Acta, Part A* **2012**, *97*, 703–710.
- (8) Clark, A. E.; Qin, C.; Li, A. D. Q. Beyond Exciton Theory: A Time-Dependent DFT and Franck-Condon Study of Perylene Diimide and Its Chromophoric Dimer. *J. Am. Chem. Soc.* **2007**, *129*, 7586–7595.
- (9) Huang, T.; Lewis, D. K.; Sharifzadeh, S. Assessing the Role of Intermolecular Interactions in a Perylene-Based Nanowire Using First-Principles Many-Body Perturbation Theory. *J. Phys. Chem. Lett.* **2019**, *10*, 2842–2848.
- (10) Pan, F.; Gao, F.; Liang, W.; Zhao, Y. Nature of Low-Lying Excited States in H-Aggregated Perylene Bisimide Dyes: Results of TD-LRC-DFT and the Mixed Exciton Model. *J. Phys. Chem. B* **2009**, 113, 14581–14587.
- (11) Seibt, J.; Winkler, T.; Renziehausen, K.; Dehm, V.; Würthner, F.; Meyer, H. D.; Engel, V. Vibronic Transitions and Quantum Dynamics in Molecular Oligomers: A Theoretical Analysis with an Application to Aggregates of Perylene Bisimides. *J. Phys. Chem. A* **2009**, *113*, 13475–13482.
- (12) Segalina, A.; Assfeld, X.; Monari, A.; Pastore, M. Computational Modeling of Exciton Localization in Self-Assembled Perylene Helices: Effects of Thermal Motion and Aggregate Size. *J. Phys. Chem.* C **2019**, *123*, 6427–6437.
- (13) Würthner, F.; Saha-Möller, C. R.; Fimmel, B.; Ogi, S.; Leowanawat, P.; Schmidt, D. Perylene Bisimide Dye Assemblies as Archetype Functional Supramolecular Materials. *Chem. Rev.* **2016**, *116*, 962–1052.
- (14) Huang, C.; Barlow, S.; Marder, S. R. Perylene-3,4,9,10-Tetracarboxylic Acid Diimides: Synthesis, Physical Properties, and Use in Organic Electronics. *J. Org. Chem.* **2011**, *76*, 2386–2407.
- (15) Angadi, M. A.; Gosztola, D.; Wasielewski, M. R. Organic Light Emitting Diodes Using Poly(Phenylenevinylene) Doped with Perylenediimide Electron Acceptors. *Mater. Sci. Eng.: B* **1999**, *63*, 191–194.
- (16) Li, C.; Wonneberger, H. Perylene Imides for Organic Photovoltaics: Yesterday, Today, and Tomorrow. *Adv. Mater.* **2012**, 24, 613–636.
- (17) Würthner, F.; Kaiser, T. E.; Saha-Möller, C. R. J-Aggregates: From Serendipitous Discovery to Supramolecular Engineering of Functional Dye Materials. *Angew. Chem., Int. Ed.* **2011**, *50*, 3376–3410
- (18) Brown, K. E.; Salamant, W. A.; Shoer, L. E.; Young, R. M.; Wasielewski, M. R. Direct Observation of Ultrafast Excimer Formation in Covalent Perylenediimide Dimers Using Near-Infrared Transient Absorption Spectroscopy. *J. Phys. Chem. Lett.* **2014**, *5* (15), 2588–2593.
- (19) Schubert, A.; Falge, M.; Kess, M.; Settels, V.; Lochbrunner, S.; Strunz, W. T.; Würthner, F.; Engels, B.; Engel, V. Theoretical Analysis of the Relaxation Dynamics in Perylene Bisimide Dimers Excited by Femtosecond Laser Pulses. *J. Phys. Chem. A* **2014**, *118* (8), 1403–1412.
- (20) Hollinbeck, S. R.; Liu, K.; Olivier, J.-H.; Grumstrup, E. M. Probing Excited State Delocalization and Charge Separation in Hierarchical Perylene Diimide Materials with Time-Resolved Broadband Microscopy. *J. Phys. Chem. C* **2024**, *128* (19), 7977–7986.
- (21) Würthner, F. Perylene bisimide dyes as versatile building blocks for functional supramolecular architectures. *Chem. Commun.* **2004**, 1564–1579.
- (22) Zhang, G.; Zhao, J.; Chow, P. C. Y.; Jiang, K.; Zhang, J.; Zhu, Z.; Zhang, J.; Huang, F.; Yan, H. Nonfullerene Acceptor Molecules for Bulk Heterojunction Organic Solar Cells. *Chem. Rev.* **2018**, *118*, 3447–3507.

- (23) Yan, C.; Barlow, S.; Wang, Z.; Yan, H.; Jen, A. K.-Y.; Marder, S. R.; Zhan, X. Non-fullerene acceptors for organic solar cells. *Nat. Rev. Mater.* **2018**, *3*, No. 18003.
- (24) Yang, Z.; Chen, X. Semiconducting Perylene Diimide Nanostructure: Multifunctional Phototheranostic Nanoplatform. *Acc. Chem. Res.* **2019**, *52*, 1245–1254.
- (25) Wirsing, S.; Hänsel, M.; Belova, V.; Schreiber, F.; Broch, K.; Engels, B.; Tegeder, P. Excited-State Dynamics in Perylene-Based Organic Semiconductor Thin Films: Theory Meets Experiment. *J. Phys. Chem. C* **2019**, *123*, 27561–27572.
- (26) Yan, Q.; Zhao, D. Conjugated Dimeric and Trimeric Perylenediimide Oligomers. Org. Lett. 2009, 11, 3426-3429.
- (27) Hauschildt, S. J.; Wu, Z.; Uersfeld, D.; Schmid, P.; Götz, C.; Engel, V.; Engels, B.; Müllen, K.; Basché, T. Excitation Localization in a Trimeric Perylenediimide Macrocycle: Synthesis, Theory, and Single Molecule Spectroscopy. *J. Chem. Phys.* **2022**, *156*, No. 044304.
- (28) Deutsch, M.; Wirsing, S.; Kaiser, D.; Fink, R. F.; Tegeder, P.; Engels, B. Geometry Relaxation-Mediated Localization and Delocalization of Excitons in Organic Semiconductors: A Quantum Chemical Study. *J. Chem. Phys.* **2020**, *153*, No. 224104.
- (29) Zheng, J.; Peng, J.; Xie, Y.; Long, Y.; Ning, X.; Lan, Z. Study of the Exciton Dynamics in Perylene Bisimide (PBI) Aggregates with Symmetrical Quasiclassical Dynamics Based on the Meyer-Miller Mapping Hamiltonian. *Phys. Chem. Chem. Phys.* **2020**, *22*, 18192–18204.
- (30) Chen, Z.; Fimmel, B.; Würthner, F. Solvent and substituent effects on aggregation constants of perylene bisimide π -stacks a linear free energy relationship analysis. *Org. Biomol. Chem.* **2012**, *10*, 5845—5855.
- (31) Grande, V.; Soberats, B.; Herbst, S.; Stepanenko, V.; Würthner, F. Hydrogen-bonded perylene bisimide J-aggregate aqua material. *Chem. Sci.* **2018**, *9*, 6904–6911.
- (32) Ronconi, F.; Syrgiannis, Z.; Bonasera, A.; Prato, M.; Argazzi, R.; Caramori, S.; Cristino, V.; Bignozzi, C. A. Modification of Nanocrystalline WO3 with a Dicationic Perylene Bisimide: Applications to Molecular Level Solar Water Splitting. *J. Am. Chem. Soc.* **2015**, *137*, 4630–4633.
- (33) Berardi, S.; Cristino, V.; Canton, M.; et al. Perylene Diimide Aggregates on Sb-Doped SnO2: Charge Transfer Dynamics Relevant to Solar Fuel Generation. *J. Phys. Chem. C* **2017**, *121*, 17737–17745.
- (34) Segalina, A.; Cerezo, J.; Prampolini, G.; Santoro, F.; Pastore, M. Accounting for Vibronic Features through a Mixed Quantum-Classical Scheme: Structure, Dynamics, and Absorption Spectra of a Perylene Diimide Dye in Solution. *J. Chem. Theory Comput.* **2020**, *16*, 7061–7077.
- (35) Segalina, A.; Aranda, D.; Green, J. A.; Cristino, V.; Caramori, S.; Prampolini, G.; Pastore, M.; Santoro, F. How the Interplay among Conformational Disorder, Solvation, Local, and Charge-Transfer Excitations Affects the Absorption Spectrum and Photoinduced Dynamics of Perylene Diimide Dimers: A Molecular Dynamics/Quantum Vibronic Approach. *J. Chem. Theory Comput.* **2022**, *18*, 3718–3736.
- (36) Negrin-Yuvero, H.; Mukazhanova, A.; Freixas, V. M.; Tretiak, S.; Sharifzadeh, S.; Fernandez-Alberti, S. Vibronic Photoexcitation Dynamics of Perylene Diimide: Computational Insights. *J. Phys. Chem. A* **2022**, *126*, 733–741.
- (37) Mukazhanova, A.; Malone, W.; Negrin-Yuvero, H.; Fernandez-Alberti, S.; Tretiak, S.; Sharifzadeh, S. Photoexcitation Dynamics in Perylene Diimide Dimers. *J. Chem. Phys.* **2020**, *153*, No. 244117.
- (38) Mukazhanova, A.; Negrin-Yuvero, H.; Freixas, V. M.; Tretiak, S.; Fernandez-Alberti, S.; Sharifzadeh, S. The Impact of Stacking and Phonon Environment on Energy Transfer in Organic Chromophores: Computational Insights. *J. Mater. Chem. C* **2023**, *11*, 5297–5306.
- (39) Malone, W.; Nebgen, B.; White, A.; Zhang, Y.; Song, H.; Bjorgaard, J. A.; Sifain, A. E.; et al. NEXMD Software Package for Nonadiabatic Excited State Molecular Dynamics Simulations. *J. Chem. Theory Comput.* **2020**, *16*, 5771–5783.
- (40) Freixas, V. M.; Malone, W.; Li, X.; Song, H.; Negrin-Yuvero, H.; Pérez-Castillo, R.; White, A.; et al. NEXMD v2.0 Software

- Package for Nonadiabatic Excited State Molecular Dynamics Simulations. J. Chem. Theory Comput. 2023, 19, 5356–5368.
- (41) Jumper, C. C.; Anna, J. M.; Stradomska, A.; Schins, J.; Myahkostupov, M.; Prusakova, V.; Oblinsky, D. G.; Castellano, F. N.; Knoester, J.; Scholes, G. D. Intramolecular Radiationless Transitions Dominate Exciton Relaxation Dynamics. *Chem. Phys. Lett.* **2014**, *599*, 23–33
- (42) van Stokkum, I. H. M.; Jumper, C. C.; Lee, T. S.; Myahkostupov, M.; Castellano, F. N.; Scholes, G. D. Vibronic and Excitonic Dynamics in Perylenediimide Dimers and Tetramer. *J. Chem. Phys.* **2020**, *153*, No. 224101.
- (43) Pope, M.; Swenberg, C. E. Electronic Processes in Organic Crystals and Polymers; Oxford University Press, 1999. https://global.oup.com/academic/product/electronic-processes-in-organic-crystals-and-polymers-9780195129632?lang=en&cc=it. (accessed April 1, 2024).
- (44) Fidder, H.; Knoester, J.; Wiersma, D. A. Optical Properties of Disordered Molecular Aggregates: A Numerical Study. *J. Chem. Phys.* **1991**, *95*, 7880–7890.
- (45) Knoester, J.; Spano, F. C. Theory of Pump-Probe Spectroscopy of Molecular. In *J-Aggregates*; World Scientific, 1996; pp 111–160.
- (46) Hestand, N. J.; Spano, F. C. Expanded Theory of H- and J-Molecular Aggregates: The Effects of Vibronic Coupling and Intermolecular Charge Transfer. *Chem. Rev.* **2018**, *118*, 7069–7163.
- (47) Cainelli, M.; Borrelli, R.; Tanimura, Y. Effect of Mixed Frenkel and Charge Transfer States in Time-Gated Fluorescence Spectra of Perylene Bisimides H-Aggregates: Hierarchical Equations of Motion Approach. *J. Chem. Phys.* **2022**, *157*, No. 084103.
- (48) Ye, J.; Sun, K.; Zhao, Y.; Yu, Y.; Lee, C. K.; Cao, J. Excitonic Energy Transfer in Light-Harvesting Complexes in Purple Bacteria. *J. Chem. Phys.* **2012**, *136*, No. 245104.
- (49) Combescot, M.; Shiau, S.-Y. Excitons and Cooper Pairs: Two Composite Bosons in Many-Body Physics; Oxford University Press, 2015.
- (50) Kühn, O. Frenkel Exciton Dynamics: A Theoretical Perspective. In *Handbook of Organic Materials for Electronic and Photonic Devices*; Elsevier, 2019; pp 259–279.
- (51) Shiau, S.-Y.; Combescot, M. A Fresh View on Frenkel Excitons. *Ann. Phys.* **2023**, 458, No. 169431.
- (52) Soler, M. A.; Bastida, A.; Farag, M. H.; Zúñiga, J.; Requena, A. A Method for Analyzing the Vibrational Energy Flow in Biomolecules in Solution. *J. Chem. Phys.* **2011**, *135*, No. 204106.
- (53) Paulino, V.; Cadena, D. M.; Liu, K.; Mukhopadhyay, A.; Roberts, S. T.; Olivier, J.-H. The Length of Molecular Tethers Can Be Used to Control the Structure and Electronic Properties of Stapled Supramolecular Polymers. *Chem. Mater.* **2022**, 34, 6518–6528.
- (54) Ashcraft, A.; Liu, K.; Mukhopadhyay, A.; Paulino, V.; Liu, C.; Bernard, B.; Husainy, D.; Phan, T.; Olivier, J.-H. A Molecular Strategy to Lock-in the Conformation of a Perylene Bisimide-Derived Supramolecular Polymer. *Angew. Chem.* **2020**, *132*, 7557–7563.
- (55) Hernandez, L. A.; Nelson, T.; Gelin, M. F.; Lupton, J. M.; Tretiak, S.; Fernandez-Alberti, S. Interference of Interchromophoric Energy-Transfer Pathways in π -Conjugated Macrocycles. *J. Phys. Chem. Lett.* **2016**, *7*, 4936–4944.
- (56) Dewar, M. J. S.; Zoebisch, E. G.; Healy, E. F.; Stewart, J. J. P. Development and Use of Quantum Mechanical Molecular Models. 76. AM1: A New General Purpose Quantum Mechanical Molecular Model. *J. Am. Chem. Soc.* **1985**, *107*, 3902–3909.